



Development and characterization of transparent and conductive InZnO films by magnetron sputtering at room temperature



J. Nicholas Alexander^{a,*}, Neville Sun^b, Richard Sun^b, Harry Efstathiadis^a, Pradeep Haldar^a

^a State University of New York Polytechnic Institute, Colleges of Nanoscale Science and Engineering, 257 Fuller Rd., Albany, NY 12203, USA

^b Angstrom Sun Technologies Inc., 31 Nagog Park, Acton, MA 01720, USA

ARTICLE INFO

Article history:

Received 26 September 2014

Received in revised form 28 January 2015

Accepted 30 January 2015

Available online 11 February 2015

Keywords:

Oxide materials

Semiconductors

Thin films

Electronic properties

Optical properties

ABSTRACT

The electrical and optical properties of InZnO for use as a transparent conducting oxide (TCO) is reported through the investigation of the concentration of indium and oxygen in the film. InZnO films (10–30 wt.% In) were deposited by magnetron sputtering without substrate heating or annealing from a ceramic ZnO and a metallic indium target. The film's properties were investigated by X-ray photoelectric spectroscopy (XPS), 4-point probe, UV–vis spectroscopy (UV–vis), spectroscopic ellipsometry, and Hall measurements. InZnO films obtained properties with low resistivity, on the order of $\sim 5.5 \times 10^{-4}$ ohm-cm, with a mobility ~ 35 cm²/V S, and carrier concentrations $\sim 3 \times 10^{20}$ cm⁻³. The band-gap ranged from 2.7 to 3.2 eV with transmission of several samples >80%. InZnO has demonstrated properties adequate for photovoltaic applications.

© 2015 Elsevier B.V. All rights reserved.

1. Introduction

Transparent conducting oxide (TCO) films have gained significant importance, due to their low film resistivity and their high transparency. These physical properties have led to the use of TCOs in applications such as flat panel displays, which consist most notably of liquid crystal displays (LCD) and organic light emitting diodes (OLED), and in thin film solar cell applications such as amorphous Si, CuInGaSe₂ (CIGS), CdTe, and CuZnSbSe [1–3].

Traditionally, many thin-film solar cells, in particular CIGS, use indium tin oxide (ITO), which is the most commonly used TCO for devices [4]. In recent years, due to unstable pricing and a relatively small indium supply, new materials have been sought to either reduce or remove indium use [5,6]. Studies were performed on new materials systems, such as ZnO doped with trivalent dopants such as boron, aluminum, gallium, and indium. The best results obtained to date with trivalent doped ZnO are with aluminum. Aluminum doped zinc oxide has been used as a TCO for CIGS in past record efficiency achieving devices, and also in past studies [7,8]. Most ZnO doped films suffer from transmission loss with high carrier concentrations, particularly in the near-infrared, in relation to similar carrier concentrations of other materials systems, such as ITO and IZO [9]. Research into the ZnO material system is heavily

ongoing due to the attractive low cost of ZnO. Co-doping of the ZnO to enhance the electrical and optical properties of the films has been an active area for new material development [10,11]. Indium zinc oxide was also investigated as a replacement for ITO and has shown improved performance on a completed CIGS device, however the amount of indium in this film is comparable to that of ITO [12].

A less investigated region in the ZnO–In₂O₃ material system that was explored in this research is the case when the Zn/(Zn + In) ratio is greater than 0.5 and less than 0.9, which consists of the Zn_xIn_{2-x}O_{x+3} type structure, which contains less indium than traditional ITO. In a previous report, InZnO deposited by pulsed laser deposition (PLD) from a ZnO and In₂O₃ target materials, good electrical measurements in this region were reported, and a decrease in carrier concentration was found until a Zn/(Zn + In) ratio of about 0.8, which could increase optical transmittance, especially in the near infrared [13]. These concentrations of indium in the film may allow for enhanced mobility without increasing carrier concentration to yield films with better transmission and electrical results. The same group that deposited the films with PLD reported improved transmission with the Zn₂In₂O₅ phase, although they did not provide any data. In another study in an effort to reduce the indium content in TCOs, deposited films of indium zinc tin oxide, which had physical properties comparable to ITO but using significantly less indium [6].

In this work, the properties of InZnO as deposited by magnetron sputtering with a Zn/(Zn + In) ratio between 0.5 and 0.9 are

* Corresponding author at: SUNY Polytechnic Institute, Colleges of Nanoscale Science and Engineering, 251 Fuller Rd., Albany, NY 122, USA. Tel.: +1 518 406 6124.

E-mail address: JAlexander@albany.edu (J.N. Alexander).

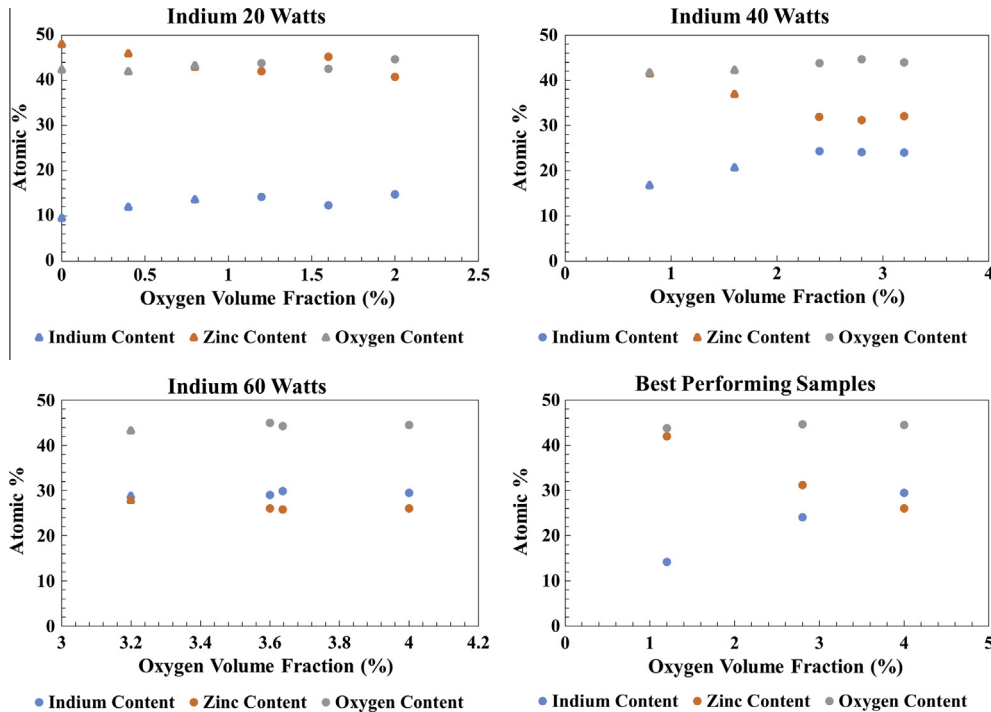


Fig. 1. Elemental composition of deposited films. For each power of indium, indium (blue), zinc (Orange), and oxygen (grey) are shown for each sample for a given oxygen volume fraction. Opaque and transparent samples are denoted by triangles and circles respectively. (For interpretation of the references to colour in this figure legend, the reader is referred to the web version of this article.)

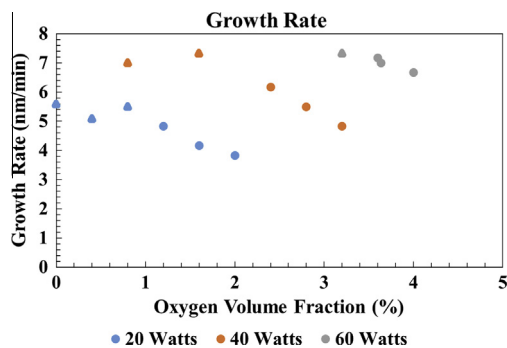


Fig. 2. Growth rate for each sample is shown with respect to its deposition power and oxygen volume fraction. Opaque and transparent samples are denoted by triangles and circles respectively.

investigated. The power of the indium target and the fraction of oxygen in argon gas (referred to as the oxygen volume fraction) were varied to deposit films with high conductivity and transparency at room temperature with different Zn/(Zn + In) ratios. The goal of this work is to deposit InZnO films with less indium than traditional ITO with good electrical and optical properties at room temperature and no post deposition anneal. The results of such will be discussed in this paper.

2. Experimental

2.1. Precursor deposition

All InZnO films in this study were deposited in an AJA International Inc. ATC physical vapor deposition reactor equipped with three, 3" diameter confocal magnetron sputtering guns and a load lock. The targets were a ceramic i-ZnO and a pure indium (99.999% purity) disks purchased from Plasmaterials Inc. The guns were positioned in a confocal alignment, allowing for simultaneous deposition of the precursor elements, and were driven independently by a 13.56 MHz rf and a DC power supply. The deposition tool was also equipped with rotating wafer stage for main-

taining film thickness and a uniform composition. The reactor was evacuated using a combination of a mechanical pump and turbomolecular pump to a base pressure of $\sim 5 \times 10^{-7}$ Torr.

The InZnO films were deposited on 1" × 3" soda-lime glass (SLG) and 1' × 1' of polished boron doped p-type Si(100) substrates with a resistivity greater than 1 ohm-cm. No special treatment was performed on the substrates before deposition except to blow them off with dry nitrogen prior to loading them in the load lock.

Before each deposition, the targets were cleaned by sputtering with the gun shutters closed to remove any excess oxides or contaminants that may have accumulated, and then run simultaneously to co-sputter at varying indium power to deposit InZnO with varying stoichiometry. The deposition power for the ZnO target was kept at 120 W, while the indium power was 20, 40, and 60 W, respectively. All the InZnO films were grown at room temperature. All other deposition parameters, such as process pressure and total gas flow rate, remained constant at 2 mT and 10 sccm (unless noted with an *, which indicates a flow rate other than 10), respectively. The gas flow mixture was varied by mixing two gases, argon gas and a 4% oxygen/argon gas, while keeping a constant sum of the flow rates.

During this study, samples were stored in a nitrogen glove box with humidity control to limit possible effects by the ambient environment. Hall measurements were performed on ~ 1 cm² glass pieces with indium contacts soldered on the four corners.

2.2. Film characterization

Film microstructural, optical, and electrical properties were investigated by a number of analytical techniques. All sample characterization discussed was performed on the InZnO films deposited on soda-lime glass substrates, with the exception of X-ray photoelectron spectroscopy, which was performed on silicon substrates.

The film thickness and optical constants of the InZnO films were obtained by using a spectroscopic ellipsometer TFProbe, SE500BA, developed by Angstrom Sun Technologies Inc. The spectroscopic ellipsometry technique allows for non-contact and non-destructive measurements of relative phase change of reflected and polarized light on any section of the film. The physical and optical properties of the InZnO films were acquired by fitting the measured ellipsometry parameters, Psi (Ψ) and Delta (Δ), to the model data using a theoretically calculated set of parameters. The parameter Ψ is defined by the following equation that includes the complex Fresnel reflection coefficients R^p and R^s , representing the reflected parallel component (P) and the perpendicular component (S) relative to the incident plane, respectively. Parameter Δ is the phase difference induced by the reflection and is obtained by analyzing the film stack and substrate in the system.

$$\rho = \frac{R^p}{R^s} = \tan \Psi \cdot e^{i\Delta} \quad (1)$$

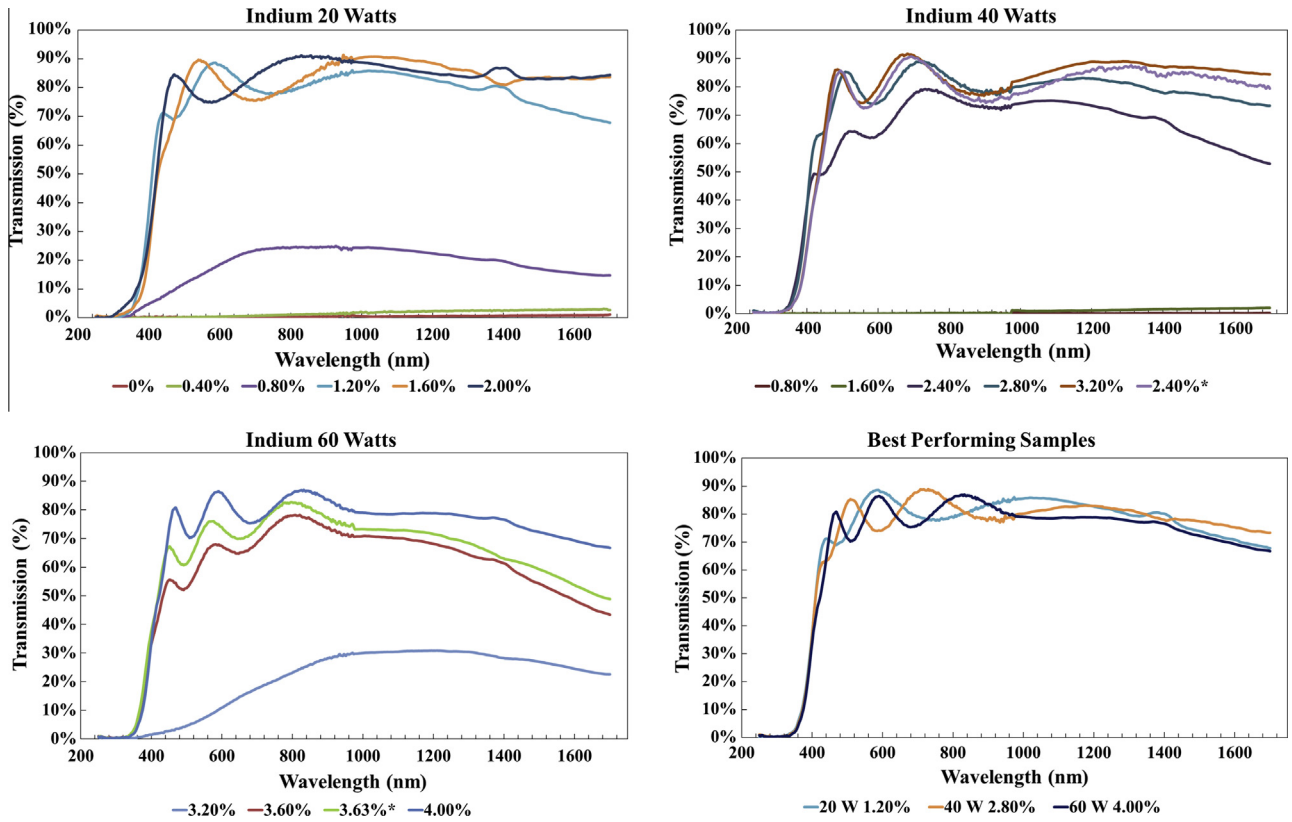


Fig. 3. Optical transmission from 250 to 1700 nm of InZnO/SLG for each sample.

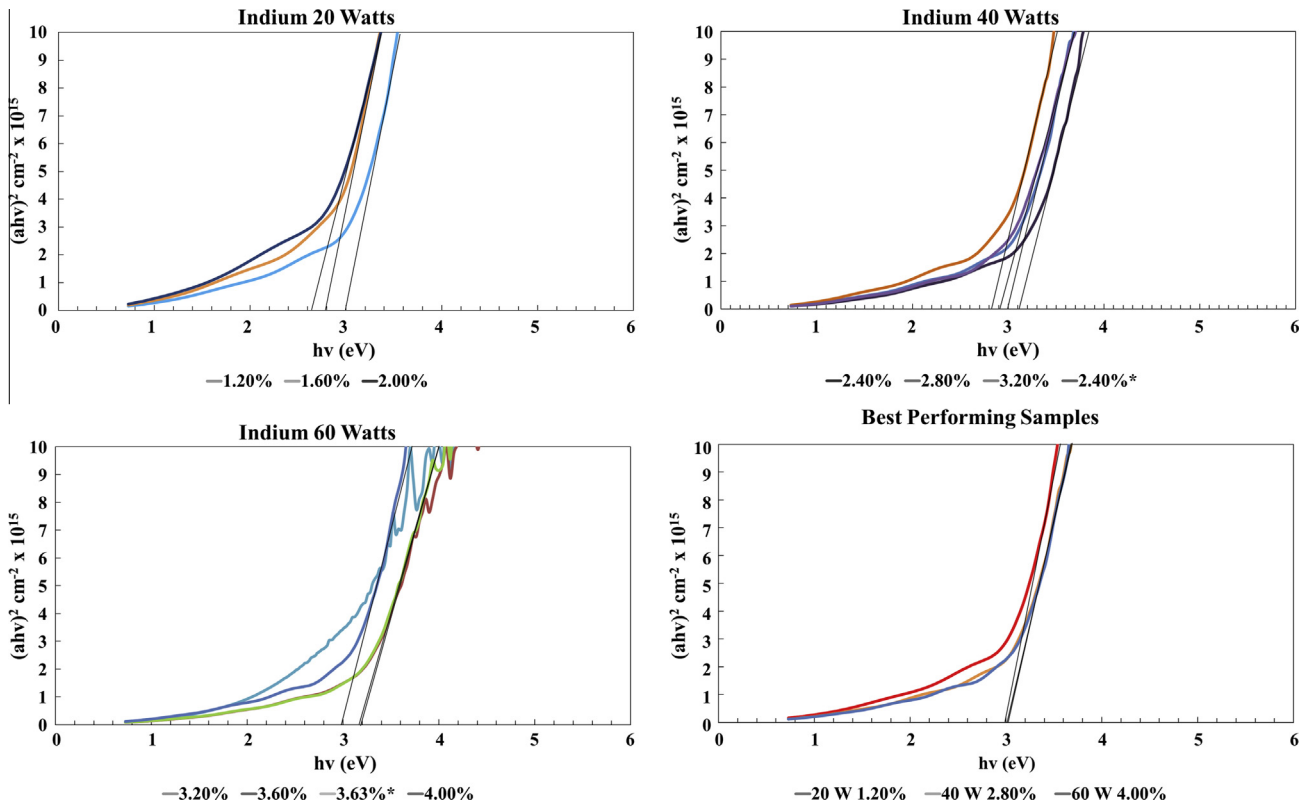


Fig. 4. Tauc plots of the transmission data from Fig. 3. Summary of band-gaps shown in Table 2 with comparison to the Tauc–Lorentz model.

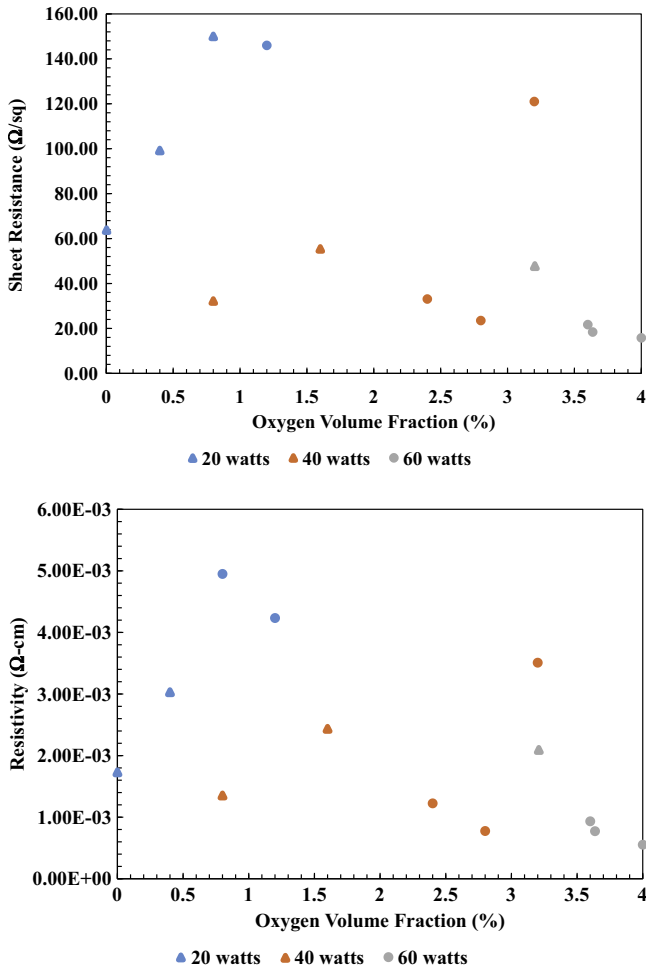


Fig. 5. Sheet resistance (top) and Bulk resistivity (bottom) as a function of oxygen volume fraction and indium power. 20 W, 40 W, and 60 W is represented by blue, orange, and grey, respectively. Opaque and transparent samples are denoted by triangles and circles, respectively. (For interpretation of the references to colour in this figure legend, the reader is referred to the web version of this article.)

The spectroscopic ellipsometry measurements were performed in the wavelength range from 250 nm to 1700 nm. All samples were measured at 65°, 70°, and 75° incident angles with 512 wavelength points. Using the TFProbe 3.3 software, a Tauc-Lorentz dispersion model was applied on the measured data sets to obtain the optical functions of the InZnO films. The imaginary part of the dielectric function ϵ_i was developed by Jessison and Modine in 1996, by multiplying the Tauc joint density of states with the Lorentz oscillator:

$$\epsilon_i(E) = \frac{AE_0C(E - E_C)^2}{((E^2 - E_0)^2 + C^2E^2)E}, \quad E > E_g, \quad (2)$$

$$\epsilon_i(E) = 0, \quad E \leq E_g,$$

where E_0 is the peak transition energy, C is the broadening term, E_g is the optical band gap, and A is proportional to the transition probability matrix element [14,15].

The real part of the dielectric function ϵ_r is calculated by Kramers-Kronig integration:

$$\epsilon_r(E) = E_{inf} + \frac{2P}{\pi} \int_{E_g}^{\infty} \frac{\xi \epsilon_i(\xi)}{\xi^2 - E^2} d\xi, \quad (3)$$

The fitting parameters in the software utilizes the variables A , C , E_0 , E_g and E_{inf} from the Tauc-Lorentz model.

When studying optical property over a very wide wavelength range, especially for TCO films, the Tauc-Lorentz dispersion is inadequate to describe the dielectric response completely. Therefore, one or more Lorentz type oscillators were added into the total dielectric function in the analysis [16]:

$$\epsilon_r = \frac{A_1\lambda^2(\lambda^2 - L_0^2)}{(\lambda^2 - L_0^2)^2 + \gamma^2\lambda^2} \quad (4)$$

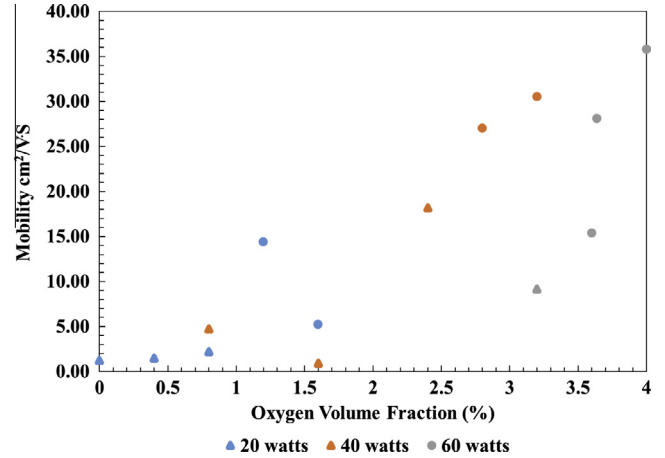


Fig. 6. Mobility as a function of oxygen volume fraction and indium power. 20 W, 40 W, and 60 W are represented by blue, orange, and grey, respectively. Opaque and transparent samples are denoted by triangles and circles, respectively. (For interpretation of the references to colour in this figure legend, the reader is referred to the web version of this article.)

$$\epsilon_i = \frac{A_1\lambda^2\gamma}{(\lambda^2 - L_0^2)^2 + \gamma^2\lambda^2} \quad (5)$$

where A_1 is the amplitude, L_0 is the central wavelength, and γ is the width of the oscillators. These three parameters are variables to be fitted using regression.

The Levenberg-Marquardt algorithm (LMA), a non-linear least-Squares method, was used for modeling. The best fitted variables can be found by minimizing χ^2 [17]:

$$\chi^2 = \frac{1}{2n - m - 1} \sum_{i=1}^n \left[(\tan\Psi_{\text{Theory}}^i - \tan\Psi_{\text{Exp}}^i)^2 + (\cos\Delta_{\text{Theory}}^i - \cos\Delta_{\text{Exp}}^i)^2 \right] \quad (6)$$

where $\tan\Psi_{\text{Theory}}$ and $\cos\Delta_{\text{Theory}}$ are the modeled values, $\tan\Psi_{\text{Exp}}$ and $\cos\Delta_{\text{Exp}}$ are measured values, m is the number of variables to be fitted, and n is the data points. The fitting process seeks to adjust those variables that could minimize the value χ^2 . Since more data points and fewer variables would make fitting results more reliable and with smaller uncertainty, variable incident angle data sets will produce higher quality ellipsometry analysis results in general.

Film thickness was also measured using an Alpha-step 200 profilometer for comparison. Composition measurements were performed with a Thermo Fisher ThetaProbe X-ray photoelectron spectroscopy (XPS). The spectrometer was equipped with a hemispherical analyzer and a monochromator and all XPS data was measured with Al $K\alpha$ X-rays (1486.6 eV) operated at 100 W and an analyzer at 45°. Hall measurements of Van der Pauw geometry were performed to measure the mobility, carrier concentrations, and sheet resistance of the films.

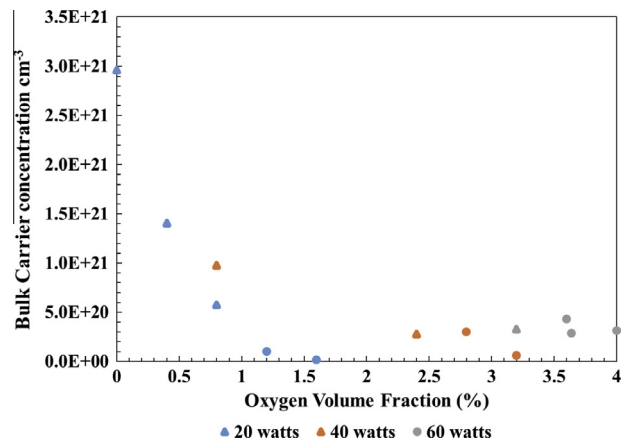


Fig. 7. Bulk Carrier concentration as a function of oxygen volume fraction and indium power. 20 W, 40 W, and 60 W are represented by blue, orange, and grey, respectively. Opaque and transparent samples are denoted by triangles and circles, respectively. (For interpretation of the references to colour in this figure legend, the reader is referred to the web version of this article.)

Table 1

Summary of all samples analyzed with Ellipsometry. Thickness and roughness from ellipsometry is shown and compared with the values obtained through profilometry. Blank cells were samples that were not optically transparent.

Sample information (indium power, oxygen %)	Roughness (nm)	Uncertainty	Thickness (nm)	Uncertainty	Total thickness (nm)	Film thickness from profilometer (nm)
20 W, 0.00%	–	–	–	–	–	335
20 W, 0.40%	–	–	–	–	–	305
20 W, 0.80%	–	–	–	–	–	330
20 W, 1.20%	5.95	±0.90	294.13	±2.05	300.08	290
20 W, 1.60%	8.95	±1.10	253.86	±1.64	262.82	250
20 W, 2.00%	9.14	±1.29	209.15	±1.64	218.29	230
40 W, 0.80%	–	–	–	–	–	420
40 W, 1.60%	–	–	–	–	–	440
40 W, 2.40%	–	–	–	–	–	370
40 W, 2.40%*	6.53	±0.95	338.87	±1.21	345.40	340
40 W, 2.80%	6.23	±1.47	361.89	±2.36	368.11	330
40 W, 3.20%	10.08	±0.81	327.96	±1.44	338.03	290
60 W, 3.20%	–	–	–	–	–	440
60 W, 3.60%	9.21	±1.20	411.55	±2.84	420.76	430
60 W, 3.63%*	6.61	±1.04	411.49	±2.39	418.09	420
60 W, 4.00%	5.51	±1.17	425.45	±2.75	430.96	440

3. Results and discussion

3.1. Film composition and growth

XPS depth profile was employed to determine film compositional characteristics. Approximately 100 nm of the top of the film were sputtered off using an ion gun inside the XPS chamber to perform the analysis without the presence of surface contamination.

In Fig. 1, the elemental concentrations of indium, zinc, and oxygen are shown for each indium deposition power for given concentrations of oxygen in 10 sccm of argon/oxygen mixture. For these films, oxygen concentration is critical for the deposition of ideal TCO films, as will be seen from the physical properties. With no oxygen in the gas mixture, films will deposit as an opaque film with a silver color, and require oxygen to become transparent.

From the results in Fig. 1, it was observed that as the oxygen volume fraction is increased, the content of oxygen and indium in the film increased in the opaque region. This was probably due to the bonding of oxygen and metallic indium atoms which continues to have this effect until the film becomes a transparent oxide. As anticipated, the higher the indium target power or higher the indium content, the more oxygen was required to produce a transparent film.

Fig. 2 shows the growth rates with respect to the indium power and their respective oxygen volume fraction in the argon–oxygen gas mixture. As oxygen is being incorporated into the film to form a more transparent oxide, the film growth rates remained almost constant. Once the film became transparent, the increase of the oxygen volume fraction started to inhibit the growth of the film, particularly in the 20 and 40 W cases. It is currently unclear if 60 W indium would follow the same trend.

Table 2

Summary of transparent samples modeled with the Tauc–Lorentz dispersion. A summary of the parameters is shown, along with a comparison of band-gap compared between the Tauc–Lorentz and Tauc Plot (Fig. 3).

Sample information (indium power, oxygen %)	A	C	E_0 (eV)	E_g (eV)	Uncertainty	E_∞	E_g (eV) (Fig. 3)
20 W, 1.20%	537.06	1.3098	2.6211	2.7987	±0.0178	2.0168	3.0
20 W, 1.60%	520.76	1.3291	2.6581	2.7064	±0.0284	2.2048	2.8
20 W, 2.00%	560.19	1.0857	2.1210	2.6807	±0.0362	2.6393	2.7
40 W, 2.40%*	168.86	2.4440	4.8748	2.6288	±0.0280	2.3969	2.9
40 W, 2.80%	153.90	4.5723	9.1444	2.6979	±0.0537	1.0664	3.0
40 W, 3.20%	148.31	4.6316	9.2630	2.6113	±0.0326	1.1839	2.8
60 W, 3.60%	237.14	5.4062	11.3455	3.1214	±0.1495	3.3896	3.2
60 W, 3.63%*	182.12	2.4242	4.9055	2.9128	±0.0491	3.3165	3.2
60 W, 4.00%	125.77	2.4404	4.9891	2.6629	±0.0264	4.1219	3.0

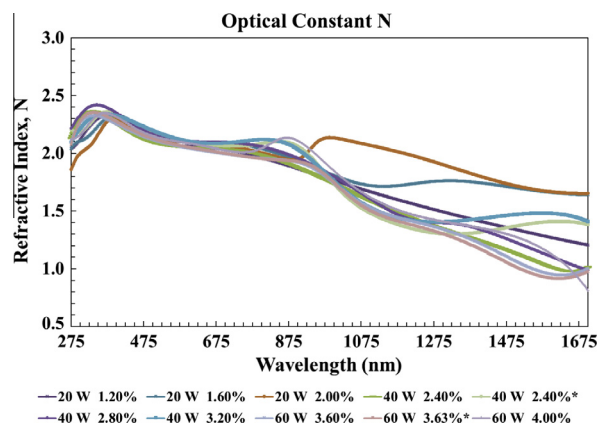


Fig. 8. Optical constant N versus wavelength from 250 to 1700 nm for optically transparent samples.

3.2. Optical transmission

For this section, transmission data were measured in the wavelength region from 250 nm to 1700 nm. It was important to include data up to this wavelength to provide insight on the near-infrared region (750–1400 nm) and a small portion of the short-wavelength infrared (1400–3000 nm), as TCO films typically start to absorb in this range [9].

Fig. 3 displays the transmission spectra for InZnO films on SLG. For each indium target power, it was found that increasing the

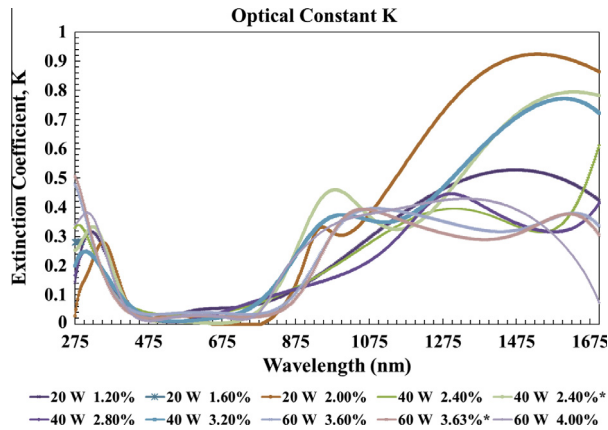


Fig. 9. Optical constant K versus wavelength from 250 to 1700 nm for optically transparent samples.

oxygen volume fraction increases the transmission. This also applies to the transparent films. The limit to the increase of the oxygen volume fraction, is that the resistivity of the films increases as the volume fraction increases. The transmission of the best performing samples were similar in the visible region were the samples 20 W 1.20% and 40 W 2.80%, but the 60 W 4.00% sample is a little less transparent. It may be possible to enhance the transmission of the 60 W sample by increasing the oxygen partial pressure. The infrared transmission of the best performing samples varies, with the best performance from the 40 W 2.80% indium sample, and the 20 W 1.20% and 60 W 4.00% samples similar to each other.

Fig. 4 shows the linear fits of the Tauc plots of the samples shown in Fig. 3. The films with poor transparent properties were not fit, as some of them exhibited properties closer to a metallic sample and are not useful for the application in mind. The band-gap varies in the transparent samples from about 2.7–3.0 eV, 2.8–3.2 eV, and 3.0–3.2 eV, for the 20 W, 40 W, and 60 W indium, respectively. Typically, the band-gap drops as the oxygen volume fraction is increased. The largest band-gap is seen in the samples that occur right after the transition to transparent samples; these samples typically do not have as good transmission along the spectrum. The conductive high transparent samples follow after those samples with a small drop in band-gap. The band-gap drops even farther as the samples transition farther into the less conductive

region. The band-gap of all the optimized samples are similar, within the 3.0–3.1 eV region.

The band-gap of the optimized films shows they are adequate for solar applications and have transmissions on par with other transparent conducting oxides that are used.

3.3. Electrical measurements

Film resistivity was measured by 4-point probe, and mobility and carrier concentration by Hall measurements were performed on square $\sim 1 \text{ cm}^2$ pieces of InZnO/SLG, with four $<0.1 \text{ cm}$ diameter indium solder balls on the sample corners.

Fig. 5 shows the sheet and bulk resistivity of the deposited films. The resistivity values of the non-transparent films were generally higher than their transparent counterparts. This is probably due to a more metallic structure of the non-transparent films. As the oxygen volume fraction was increased, the resistivity of the non-transparent samples was increased until they transitioned and became transparent. After becoming transparent, there is a decrease in resistivity. The samples now are transparent and conductive for a range of oxygen partial pressures until resistivity starts to increase significantly with increasing oxygen partial pressure. This can be seen most clearly in the 40 W sample set. This can also be seen in the 20 W indium samples, though the two samples after the 1.20% oxygen volume fraction sample were omitted due to their resistivity values being much larger than the others, at 3300 ohm-square for the 1.60% and $>1 \text{ M}\Omega/\square$ for 2.00% oxygen volume fraction samples. Bulk resistivity values on the order of $10^{-4} \Omega\text{-cm}$ were obtained with 40 W 2.80% and 60 W 4.00% indium, and nearly obtained with 20 W 1.20%.

Fig. 6 shows mobility with respect to oxygen volume fraction and indium deposition power. Low mobility is seen for 20 W indium in the non-transparent samples. As the film transitions to a transparent conducting oxide film, the mobility sharply increases until the film becomes over-saturated with oxygen and the mobility decreases. The trend is similar with 40 W and 60 W samples, which exhibit low mobility in the non-transparent region but have increases in mobility in the optimal levels. The decrease in mobility due to over-saturation of oxygen is not seen in the 40 W and 60 W samples, but is expected to occur if the oxygen volume fraction is increased to the over-saturation levels seen in the 20 W samples. The highest mobility observed in this study was the 4% oxygen volume fraction in the 60 W set.

Table 3
Summary of Optical constants N and K for all samples at 400, 633, 800, and 1500 nm.

Sample information (indium power, oxygen %)	Optical constant							
	400 nm		633 nm		800 nm		1500 nm	
	N	K	N	K	N	K	N	K
20 W 0.00%	1.8919	1.2891	2.3916	1.4786	2.6443	1.4157	2.6216	2.4959
20 W 0.40%	1.6876	0.8096	1.8929	0.9872	2.0834	0.9937	1.9206	1.7137
20 W 0.80%	2.0682	0.2328	1.9901	0.1429	1.9541	0.1688	1.3354	0.9961
20 W 1.20%	2.3042	0.1164	2.0538	0.0523	1.9623	0.0782	1.3405	0.5263
20 W 1.60%	2.3314	0.1826	2.098	0.0528	2.0399	0.0555	1.7011	0.8305
20 W 2.00%	2.2977	0.1312	2.0928	0.0074	2.0046	0.0130	1.7190	0.9210
40 W 0.80%	2.3719	2.0528	3.2475	2.0299	3.5030	1.8308	3.4698	3.3364
40 W 1.60%	2.2728	0.8340	2.3896	0.9225	2.5217	0.8652	2.4000	1.7583
40 W 2.40%	2.2669	0.0859	2.0503	0.0328	1.9863	0.0833	1.1369	0.3238
40 W 2.40%*	2.3404	0.1146	2.0852	0.0036	2.0844	0.0780	1.3695	0.7408
40 W 2.80%	2.3505	0.0898	2.0988	0.0260	2.0578	0.0924	1.2300	0.3341
40 W 3.20%	2.3263	0.0962	2.0906	0.0167	2.1188	0.1048	1.4695	0.7283
60 W 3.20%	2.1991	0.2860	2.2112	0.2895	2.1250	0.2453	3.5124	0.0133
60 W 3.60%	2.2553	0.0740	2.0271	0.0402	1.9574	0.0407	1.0681	0.3284
60 W 3.63%*	2.2766	0.0640	2.0345	0.0281	1.9538	0.0304	1.0192	0.3205
60 W 4.00%	2.3157	0.0908	2.0679	0.0307	2.0417	0.0813	1.2775	0.3762

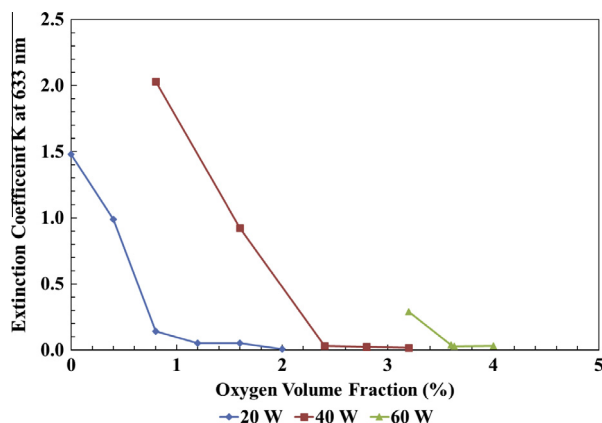


Fig. 10. Extinction Coefficient K at 633 nm for all samples. Each indium deposition power is represented by a separate line.

Fig. 7 shows the carrier concentration of electrons in the film for a given oxygen volume fraction at each indium deposition power. The trend here is as anticipated: that the carrier concentration will drop as oxygen volume content increases. As oxygen content increases, oxygen vacancies which were previously donating electrons to the system are being filled. For each increase in indium power, there is an increase in carrier concentration, which also can be supported by carriers coming from interstition metal ion impurities or doping ions. Although having a higher carrier concentration will result in films with better resistivity values, an increase in carrier concentration can also contribute to reductions in transmission, particularly in the near-infrared.

3.4. Ellipsometry analysis and results

All ellipsometry data were analyzed with the Tauc–Lorentz Model. The results are summarized in Table 1.

From Table 1, it can be seen that the thickness measurements obtained with both thin film measurement techniques are consistent. Furthermore, the roughness information, which is related to the deposited film quality, can also be obtained with the spectroscopic ellipsometry technique and is reported in the table.

Several modeled parameters are given in Table 2. With the Tauc–Lorentz dispersion, optical band gap could be readily obtained with a small uncertainty related to the three sigma output at 95% confidence from the mathematical regression. The band gap information is essential in optimizing film design and in evaluation of the film's performance. Samples 20 W 1.20%, 40 W 2.80%, and 60 W 4.00% had the best performance electrically and are shown to have a band-gap of 2.7–2.8 eV from the Tauc–Lorentz method. Optical transmission measurements confirmed the criteria for optimization of both processing parameters and composition design. For comparison, the band-gaps from the Tauc plots (Fig. 3) are included in the table. It can be seen that typically the Tauc plots yield higher band-gaps than the Tauc–Lorentz method. Possibly, because the Tauc–Lorentz parameters are calculated from ellipsometry data, they may be more sensitive to phase information, unlike Tauc plots, which are generally used for estimated band-gap and are fit from the transmission data. They both exhibit the same trends as discussed previously, with decreasing band-gap with increasing oxygen content in the films.

Optical constants, refractive index (N), and extinction coefficient (K), were plotted in Figs. 8 and 9 for the selected samples. Fig. 8 shows that the transparent samples all exhibit a similar refractive index in the visible region. Refractive index in the

near-infrared region is higher in samples with higher resistivity, with the highest refractive index observed for the 20 W 2.00% oxygen sample with resistivity on the order of $M\Omega$ -cm. From Fig. 9, the K plot for these samples exhibits typical characteristics of TCO film, i.e. low absorption in the visible wavelength range. N and K values at the 400, 633, 800, and 1500 nm wavelength are listed in Table 3 for comparison of each film obtained at different deposition conditions (see Fig. 10 for K values at 633 nm).

To examine the effects of the processing parameters on absorption behavior of the films, extinction coefficients K at a wavelength of 633 nm was plotted against the volume fraction of Oxygen at three different levels of sputtering power for indium. It can be seen that (1) absorption of films decreases with increasing oxygen concentration in the argon–oxygen mixture at each sputtering power; (2) relatively higher oxygen concentration is needed to achieve smaller absorption at higher sputtering power.

4. Discussion

For solar cell applications where cost to performance is of major concern, the material and processing costs need to be balanced with the performance of the material. InZnO deposited in this study through a relatively simple room temperature deposition with no complicated steps has yielded electrical and optical transmittance which is on par with standard TCO materials such as ITO and AZO.

The films produced in this study use considerably less indium than typical ITO films, and were shown to have the ability to deposit with good electrical properties without annealing, on par with many reports on ITO [18,19]. They have been shown to have properties similar to AZO, although AZO currently remains a cheaper alternative [20,21]. In comparison to other TCOs, transmission is similar, though some of the samples exhibited transmission in the infra-red region that is greater than reported for ITO and AZO, which is beneficial for photovoltaic applications [9,22]. Future directions for this work include investigation of devices on CIGS in comparison with other TCO materials, and use with alternative CdS buffer developed in previous work [8].

5. Conclusions

InZnO films, deposited by magnetron co-sputtering at room temperature, were studied as a potential replacement material for typical TCO materials commonly used in research and commercial applications. The effects of the oxygen volume fraction in the flow gas on the electrical and optical properties of InZnO with no post deposition annealing were studied. InZnO can be deposited on par with other leading TCO materials with resistivity values as low as $\sim 5.5 \times 10^{-4}$ and optical transmission greater than 80% in the visible spectrum through oxygen optimization. Films with higher indium content were able to achieve high mobility values greater than $30 \text{ cm}^2/\text{V S}$ with carrier concentrations low enough to maintain a high near-infrared transmission. The band-gap was found to be acceptable for photovoltaic applications ranging from 2.7 to 3.2 eV. Indium consumption compared to ITO have been considerably reduced without sacrificing film properties. InZnO deposited under these conditions has thus demonstrated properties that are appropriate for use as the transparent conduction oxide for photovoltaic applications.

Acknowledgement

This work is partially funded by the United States Department of Energy (DOE) Award Number: DE-EE0004947.

References

- [1] H. Liu, V. Avrutin, N. Izyumskaya, Ü. Özgür, H. Morkoç, *Proc. Int. Sch. Phys.* 48 (2010) 458–484.
- [2] A. Chandra, G. Anderson, S. Melkote, W. Gao, H. Haitjema, K. Wegener, *CIRP Ann. Manuf. Technol.* 63 (2014) 797–819.
- [3] J.A. Stoke, J.D. Beach, W.C. Bradford, T.R. Ohno, *Thin Solid Films* 562 (2014) 254–259.
- [4] K. Ellmer, *Nat. Photon.* 6 (2012) 809–817.
- [5] T. Minami, *Semicond. Sci. Technol.* 20 (2005) S35–S44.
- [6] M. Putri, C.Y. Koo, J. Lee, J. Kim, H.Y. Lee, *Thin Solid Films* 559 (2014) 44–48.
- [7] P. Jackson, D. Hariskos, E. Lotter, S. Paetel, R. Wurz, R. Menner, W. Wischmann, M. Powalla, *Prog. Photovolt. Res. Appl.* 19 (2011) 894–897.
- [8] J.N. Alexander, S. Higashiya, D. Caskey Jr, H. Efstathiadis, P. Haldar, *Sol. Energy Mater. Sol. Cells* 125 (2014) 47–53.
- [9] G. Gonçalves, E. Elangovan, P. Barquinha, L. Pereira, R. Martins, E. Fortunato, *Thin Solid Films* 515 (2007) 8562–8566.
- [10] S. Jeong, J. Park, B. Lee, *J. Alloys Comp.* 617 (2014) 180–184.
- [11] S. Park, J. Koh, *Ceram. Int.* 40 (2014) 10021–10025.
- [12] J.D. Perkins, T. Gennett, J.E. Leisch, R. Sundaramoorthy, I.L. Repins, M.F.A.M. Van Hest, D.S. Ginley, in: 35th IEEE PVSC, 2010, pp. 989–991.
- [13] N. Naghavi, L. Dupont, C. Marcel, C. Maugy, B. Laïk, A. Rougier, C. Guéry, J.M. Tarascon, *Electrochim. Acta* 46 (2001) 2007–2013.
- [14] G.E. Jellison, F.A. Modine, *Appl. Phys. Lett.* 69 (1996) 371–374.
- [15] H.G. Thompson, E.A. Irene, *Handbook of Ellipsometry*, William Andrew Inc, Norwich, New York, 2005.
- [16] R. Hummel, *Electronics Properties of Materials*, third ed., Springer-Verlag, Berlin, Heidelberg, New York, 2000.
- [17] W. Press, S. Teukolsky, W. Vetterling, B. Flannery, *Numerical Recipes in C: The Art of Scientific Computing*, second ed., Press Syndicate of the University of Cambridge, Cambridge, 1992.
- [18] J. Hotovy, J. Hüpkas, W. Böttler, E. Marins, L. Spiess, T. Kups, V. Smirnov, I. Hotovy, J. Kováč, *Appl. Surf. Sci.* 269 (2013) 81–87.
- [19] T. Koida, H. Fujiwara, M. Kondo, *J. Non-Cryst. Solids* 354 (2008) 2805–2808.
- [20] T. Ghosh, D. Basak, *Sol. Energy* 96 (2013) 152–158.
- [21] Q. Shi, K. Zhou, M. Dai, H. Hou, S. Lin, C. Wei, F. Hu, *Ceram. Int.* 39 (2013) 1135–1141.
- [22] K.M. Yu, M.A. Mayer, D.T. Speaks, H. He, R. Zhao, L. Hsu, S.S. Mao, E.E. Haller, W. Walukiewicz, *J. Appl. Phys.* 111 (2012). 123505-123505-5.